Am J Cancer Res 2023;13(12):5934-5949
www.ajcr.us /ISSN:2156-6976/ajcr0153801

Original Article

MMP11 and MMP14 contribute to the interaction between castration-resistant prostate cancer and adipocytes

Bing Tan[1,2,3], Xiaoyu Zheng[4], Xiaoqin Xie[5], Yirong Chen[1], Yuehua Li[1], Weiyang He[3]

[1]Department of Urology, University-Town Hospital of Chongqing Medical University, Shapingba District, Chongqing 401331, China; [2]Medical Sciences Research Center, University-Town Hospital of Chongqing Medical University, Shapingba District, Chongqing 401331, China; [3]Department of Urology, The First Affiliated Hospital of Chongqing Medical University, Yuzhong District, Chongqing 400016, China; [4]School of Clinical Medicine, Chongqing Medical and Pharmaceutical College, Shapingba District, Chongqing 401331, China; [5]Department of Clinical Laboratory, Chongqing Blood Center, Jiulongpo District, Chongqing 400015, China

Received October 6, 2023; Accepted December 10, 2023; Epub December 15, 2023; Published December 30, 2023

Abstract: Previous studies have demonstrated that adipocytes promote prostate cancer (PCa) cell progression, which facilitates the development of PCa into castration-resistant prostate cancer (CRPC); however, the underlying mechanisms are still not fully understood. Matrix metalloproteinases (MMPs) are a group of proteases responsible for the degradation of extracellular matrix (ECM) and the activation of latent factors. In our study, we detected that MMP11 expression was increased in PCa patients and that a high level of MMP11 was correlated with poor prognosis. Furthermore, siRNA knockdown of MMP11 in CRPC cells not only blocked the delipidation and dedifferentiation of mature adipocytes but also reduced the lipid uptake and utilization of CRPC cells in a cell co-culture model. The number of mitophagosomes and the expression level of Parkin were increased in MMP11-silenced CRPC cells. Moreover, we found that simultaneous downregulation of MMP14 and MMP11 expression may benefit patient survival. Indeed, MMP11/14 knockdown in CRPC cells significantly decreased lipid metabolism and cell invasion, at least partly through the mTOR/HIF1α/MMP2 signaling pathway. Importantly, MMP11/14 knockdown dramatically delayed tumor growth in a xenograft mouse model. Consistently, the decreased lipid metabolism, Ki67 and MMP2 expression, as well as the increased Parkin level were also confirmed in in vivo experiments, further demonstrating the mechanisms responsible for the tumor-promoting effects of MMP11/14. Collectively, our study elucidated the role of MMP11 and MMP14 in the bidirectional crosstalk between adipocytes and CRPC cells and provided the rationale of targeting MMP11/14 for the treatment of CRPC patients.

Keywords: Castration resistant prostate cancer, adipocyte, matrix metalloproteinase, mitophagy, lipid metabolism

Introduction

Prostate cancer (PCa) is a disease with high prevalence and mortality, and multidrug resistance and distant organ metastasis are the leading causes of PCa-related death in men worldwide [1]. PCa incidence and progression are associated with obesity according to recent epidemiological studies, and obese men undergoing radical prostatectomy are at higher risk for PCa progression and aggressiveness, as well as biochemical recurrence [2]. Additionally, obesity increases the risk of PCa progression to castration-resistant prostate cancer (CRPC), metastasis and CRPC-specific mortality [3]. It has been well documented that the dynamic interactions between CRPC cells and the tumor microenvironment (TME) are one of the driving forces of cancer progression. The TME comprises not only noncellular components such as the extracellular matrix (ECM) and soluble factors such as extracellular vesicles, chemokines, and cytokines, but also noncancerous host cells, including immune cells, endothelial cells, fibroblasts, and adipocytes [4]. Adipocytes in the tumor periphery exhibit significant phenotypic changes, including a decreased lipid content and the expression of adipocyte markers, while

a high expression of proinflammatory cytokines and ECM-related molecules [5]. However, how adipocytes communicate with CRPC cells and how they contribute to cancer progression remain elusive.

A key component of tumor invasion and metastasis is matrix metalloproteinases (MMPs) which degrade protein components in the ECM and impair tissue barrier integrity. Based on their substrates and structural homology, MMPs are classified into six classes: collagenases, gelatinases, matrix degraders, matrilysins, furin-activated MMPs, and other secreted MMPs [6]. MMP11 is a secreted protein that regulates numerous physiological processes and signaling pathways, as well as alters cellular behavior, thereby playing a key role in the TME [7]. Previous studies have linked high levels of MMP11 to advanced tumor stage and the poor prognosis of PCa patients [8, 9]. It has also been reported that MMP11 promotes malignancy by inhibiting apoptosis and promoting migration and invasion [10, 11]. Nevertheless, the functional mechanisms of MMP11 are not fully understood. In addition to MMP11, MMP14 has also been reported to be upregulated in PCa and to promote cancer cell invasion and metastasis in obese patients [12]. Studies using in vivo mouse model reveal that membrane-associated MMP14 promotes breast cancer growth via mTOR-dependent activation of hypoxia inducible factor 1α (HIF1α) and regulates ATP production through its intracytoplasmic tail domain via enhancing aerobic glycolysis in macrophages [13, 14]. Furthermore, MMP14 may partially favor the limitation of MMP11 activity in vitro [15], though in vivo validation is required. Since MMP14 is localized in the cell membrane while MMP11 is soluble in the TME, we hypothesize that there may exit an MMP-dependent molecular network that reciprocally regulates cellular function and the dysregulation facilitates the development of advanced-stage CRPC.

Mitochondria are the primary energy-producing organelles and the main source of reactive oxygen species (ROS). Although mitochondrial lipid catabolism is critical in supplying ATP to breast cancer cells for their survival [16], emerging evidence has shown that the surrounding adipocytes can provide PCa cells with free fatty acids (FFAs), while the metabolically reprogrammed cancer cells have greater viability [12]. Mitochondrial dysfunction manifests as irregular morphology, insufficient ATP production, as well as an increased production of ROS and oxidative damage to lipids, proteins, and nucleic acids. In response to oxidative stress, mitophagy enables the elimination of excess and damaged mitochondria to prevent detrimental effects, thereby restoring cancer cell homeostasis [17].

Here, we examined MMP11 and MMP14 expression in clinical specimens and explored the relationship between MMP11/14 and PCa patient overall survival. Furthermore, a cell coculture model and metabolomics analysis were utilized to confirm the role of MMP11/14 in CRPC cell lipid metabolism. We found that CRPC cell mitophagy is stimulated by silencing MMP11/14, leading to attenuated tumor growth. The reduction in tumor lipid metabolism and invasiveness is probably mediated by the mTOR/HIF1α/MMP2 pathway. In conclusion, this study demonstrated the growth-promoting role of MMP11/14 and elucidated the mechanism underlying the inhibition of lipid metabolism and the promotion of mitophagy. Our findings also shed light on targeting MMP11/14 for the treatment of CRPC patients.

Materials and methods

TCGA data processing

Data from 52 normal prostate and 501 tumor prostate tissues were downloaded from The Cancer Genome Atlas (TCGA) database to analyze gene expression profiles and the overall survival probabilities of the corresponding patients based on the expression of single genes and two-gene combinations (https://portal.gdc.cancer.gov/).

Clinical tissue specimens

Tissue specimens from clinical patients were obtained from the University-Town Hospital of Chongqing Medical University. Pathological examination was performed to determine the tissue classification. All patients involved in this study provided informed consent. This study was conducted in strict compliance with the 1964 Declaration of Helsinki and its later amendments or comparable ethical standards and was approved by the Ethics Committee of

University-Town Hospital of Chongqing Medical University.

Adipocyte differentiation, cell coculture and siRNA transfection

Cells were incubated with 5% CO_2 at 37°C. Differentiation of 3T3-L1 preadipocytes (FuHeng Bio, China) was induced by incubation for two days in differentiation medium (DMEM high-glucose, 10% FBS, 1% penicillin/streptomycin, 10 μg/mL insulin, 0.5 μmol/L isobutylmethylxanthine, 1 μmol/L rosiglitazone, 1 μmol/L dexamethasone), and the cells were then treated with fresh culture medium (containing 10 μg/mL insulin) for another two days. The medium was changed back to fresh complete medium every two days until fourteen days of full differentiation was achieved.

Human CRPC cell lines (Du145, PC3 and C42B) were donated by Dr. YB Zheng from Chongqing Medical University and maintained in DMEM. A Transwell system with 0.4 μm pores (Millipore, US) was adopted to coculture adipocytes and CRPC cells. A total of 5×10^4 CRPC cells were seeded in the upper chamber, with mature adipocytes seeded in the lower chamber; alternatively, mature adipocytes were seeded in the upper chamber, with 2×10^5 CRPC cells seeded in the lower chamber (detailed in **Figure 2**). The cocultures were then incubated for 72 hours.

Effective siRNAs (Biomics, China) were selected after verification by western blotting and transfected into cancer cells using Lipofectamine 2000 (Invitrogen, US) according to the manufacturer's specifications. The sequences of the siRNAs are listed in Table S1. The culture medium was replaced with basal medium after 48 hours of transfection.

Reverse transcription (RT) and quantitative PCR (qPCR)

Total RNA was extracted from cells and tissues using TRIzol reagent. The concentrations of RNA in the samples were measured at an absorbance of 260 nm. SuperScript RT Master Mix and SYBR GreenER qPCR SuperMix (Invitrogen, US) were used for the RT and qPCR steps. The primers for all tested genes are summarized in Table S1, and GAPDH expression was used as an internal reference. The experiment was performed at least three times.

Western blotting

Total protein from cells was extracted using RIPA buffer supplemented with protease and phosphatase inhibitors (PMSF, NaF and Na_3VO_4) (Roche, Switzerland). Protein concentrations were measured by a BCA kit (P0010, Beyotime, China). Proteins (40 μg samples) were separated by electrophoresis and transferred to a PVDF membrane. The primary and secondary antibodies used are listed in Table S2. Finally, signals were visualized using an extreme high-sensitivity ECL kit (P0018FM, Beyotime, China).

Immunofluorescence

Cultured cells were grown on glass coverslips and exposed to different treatments. After 48 hours of culture, the cells were fixed with 4% paraformaldehyde, permeabilized with 0.1% Triton X-100, and blocked with 5% goat serum. Then, the cells were washed with phosphate-buffered saline (PBS) and incubated in dilution buffer with a primary antibody (Table S2) overnight at 4°C. Subsequently, the cells were stained with the corresponding fluorochrome-conjugated secondary antibody (Table S2) and DAPI (C04002, Bioss, China). Images were acquired using fluorescence microscopy (Zeiss, Jena, Germany).

Cell invasion assay

A Transwell assay was employed to estimate the invasion ability of cells. The membranes in the upper chambers were precoated with 5% Matrigel (BD Biosciences, US). Then, 4×10^4 cells were added to the upper chambers with 8 μm pore membranes (Millipore, US) and cultured in 500 μL of serum-free medium. Well-differentiated adipocytes were cultured in the lower chambers containing serum. The invaded cells were stained with crystal violet and counted under a light microscope.

Metabolite profiling

The data for metabolomic analysis were acquired with an LC-MS/MS system coupled to a quadrupole Orbitrap mass spectrometer (Q Exactive Orbitrap, Thermo Fisher Scientific, US). Metabolites with significant differences in abundance were screened and analyzed by principal component analysis (PCA), orthogonal partial least squares discriminant analysis

(OPLS-DA), hierarchical clustering heatmap analysis, volcano plot analysis, metabolic pathway classification and Kyoto Encyclopedia of Genes and Genomes (KEGG) enrichment analysis. A variable importance in projection (VIP) value of greater than 1 and a *p* value of less than 0.05 were used as the selection criteria.

Oil Red O staining

Cultured adipocytes were stained with an Oil Red O Staining Kit (C0157M, Beyotime, China). Working solutions were prepared according to the manufacturer's instructions. After 10 minutes of staining, the cells were washed with PBS and photographed.

ELISA

MMP11 protein concentrations in the culture medium of CRPC cell lines were measured by ELISA kits (YS01645B, YaJiBio, China). Then, MMP11 protein concentrations were determined with a double antibody sandwich assay in microplates coated with purified antibody. In accordance with the manufacturer's instructions, the absorbance was measured at 450 nm.

Transmission electron microscopy

The morphology of mitophagosomes and mitochondria was evaluated by transmission electron microscopy (Philips Medical Systems, Eindhoven, Netherlands). Cells were first fixed with 2.5% glutaraldehyde and 1% osmium tetroxide and were then dehydrated in an ethanol and acetone gradient. Next, samples were embedded in araldite, sliced into ultrathin sections and stained with 3% lead citrate-uranyl acetate, and images were acquired.

BODIPY staining

Adipocytes in the cell coculture model and frozen sections from tumor tissues were fixed with 4% paraformaldehyde for 30 minutes and permeabilized with 0.1% Triton X-100 for 30 minutes. After blocking with 1% BSA for 60 minutes, adipocytes were incubated with 1:1000 BODIPY 493/503 fluorescent dyes (ajci70160, Amgicam, China) to label accumulated lipids. Lipid droplets were further examined using a fluorescence microscope (Zeiss, Jena, Germany).

Histological staining

Paraffin-embedded mouse tumors, PCa tissue sections and adjacent normal prostate tissue sections were deparaffinized and rehydrated, and endogenous peroxidase activity was quenched with 3% hydrogen peroxide. Next, the sections were incubated with bovine serum albumin for 30 min. Primary antibodies (Table S2) were diluted in PBS and incubated with the sections at 4°C overnight. An immunohistochemical detection kit (PV6000, ZSGB-bio, China) was applied to detect protein signals. As a negative control, sections were incubated with PBS instead of a primary antibody. The signal intensity was used to score staining as follows: no staining =0, weak staining =1, medium staining =2, and strong staining =3. The percentage of positive cells was scored as follows: staining in 0% of cells =0, < 5% of cells =1, 5%-50% of cells =2, and > 50% of cells =3. Positive staining was defined as a sum of these two scores equal to or greater than 3. In addition, histopathological changes were detected by staining rehydrated tissue sections with hematoxylin and eosin (HE).

Cell line-derived xenografts

Du145 cells (2×10^6) were suspended in 100 μL of PBS and were then subcutaneously injected into male nude mice at the region of the inguinal canal containing adipose tissue. Six-week-old male mice were divided into the indicated groups (n=9 mice/group). The tumor volumes were calculated at four time points with the formula 3.14/6 × length × width × height, and tumor weights were evaluated at the termination of the experiment. After all mice were sacrificed, transplanted tumor tissues were utilized to perform HE, immunohistochemical and BODIPY staining. The procedures for the in vivo animal experiment were approved by the Ethics Committee of University-Town Hospital of Chongqing Medical University.

Data and statistical analysis

ImageJ software was used to analyze image data. SPSS 24.0 and GraphPad Prism 9 software were employed for statistical analyses. Unpaired Student's t test was adopted for comparisons between two groups, while one-way ANOVA followed by Tukey's multiple comparison test was used for comparisons among multiple

groups. Analysis of gene expression in TCGA was performed using the Wilcoxon rank-sum test, and survival analysis was conducted using the Kaplan-Meier method and the log-rank test. Three independent experiments were performed for each assay, with $P < 0.05$ indicating a significant difference.

Results

High MMP11 expression level was correlated with the poor prognosis of PCa patients

By using data from the TCGA database, we analyzed the expression level of MMP11 in 52 normal prostate and 501 tumor samples and found a higher MMP11 level in tumors than in normal tissues (**Figure 1A**). In addition, PCa patients with high MMP11 expression had a lower survival rate (**Figure 1B**). To further confirm MMP11 protein expression, we examined PCa and adjacent normal prostate sections by immunohistochemistry (IHC). As shown in **Figure 1C**, we observed a distinctly higher expression of MMP11 in cancerous tissues than in control normal tissues.

Knockdown of MMP11 in CRPC cells inhibited lipid metabolism and prevented mature adipocyte lipolysis in a cell co-culture model

It has been reported that tumor cells can interact with adipocytes in the TME, possibly in a paracrine manner. To study the bidirectional crosstalk between CRPC cells and adipocytes, we chose Du145 and PC3 cell lines, as they had higher endogenous MMP11 level than adipocytes did (Figures S1 and S2), to establish a cell co-culture model in vitro (**Figure 2A** and **2E**). Specifically, Du145 and PC3 cells were co-cultured with fully differentiated 3T3L1 preadipocytes. The expression level of MMP11 in Du145 and PC3 cells was manipulated by siRNA transfection, and the knockdown of MMP11 was verified by western blotting and ELISA of the cell lysate and supernatant medium, respectively (Figure S3A and S3B). We found silencing MMP11 in CRPC cells suppressed the delipidation in mature adipocytes leading to a higher percentage of adipocyte area (**Figure 2B**). Similarly, BODIPY lipid staining showed that the average size of lipid droplets in MMP11 knockdown group was greater than that in the control group, while the cells in the control group displayed a fusiform shape (**Figure 2C**). Furthermore, RT-qPCR revealed that co-culture with MMP11 knockdown CRPC cells led to a strong elevation in the mRNA levels of three terminal differentiation markers: fatty acids (FAs) binding protein 4 (FABP4), peroxisome proliferator-activated receptor gamma (PPARγ), and CCAAT/enhancer-binding protein alpha (C/EBPα), in adipocytes (**Figure 2D**). Moreover, we observed a dramatic decrease in lipid uptake, utilization, and anabolism markers, such as the FAs transporter CD36, rate-limiting enzyme carnitine palmitoyltransferase 1 (CPT1) for FAs oxidation and FAs synthase (FASN), in MMP11-silenced CRPC cells compared to control cells (**Figure 2F**). These results suggest that MMP11 is required for the active interaction between CRPC cells and adipocytes.

Silencing MMP11 increased mitophagy in CRPC cells

In mitochondria, FAs undergo complete oxidation to produce ATP. Under nutrient deprivation, mitophagy is induced to eliminate defective or excess mitochondria via lysosomal degradation [17]. We then used electron microscopy to examine the effect of MMP11 knockdown on mitochondria and observed increased deformed mitochondria and morphological changes, the characterization of mitophagy (**Figure 3A**). Parkin-dependent mitophagy is a major mechanism for eliminating dysfunctional mitochondria [18]. Interestingly, immunofluorescence staining revealed an increase in Parkin accumulation in MMP11-silenced Du145 and PC3 cells (**Figure 3B**), suggesting that MMP11 is important in maintaining metabolic integrity and homeostasis in CRPC cells through the Parkin-dependent mitophagy pathway.

The mTOR/HIF1α/MMP2 pathway was involved in the inhibition of lipid metabolism and invasion of CRPC cells induced by MMP11 and MMP14 silencing

Since a previous study has suggested that MMP14 may protect cells from abnormal MMP11 activity [15], we first collected MMP14 expression data from the TCGA and found a lower MMP14 expression in prostate tumors than in normal tissues (**Figure 4A**). Consistently, lower MMP14 staining scores was detected in PCa than in normal tissues by IHC (**Figure 4D**). Furthermore, the low MMP14 expression was

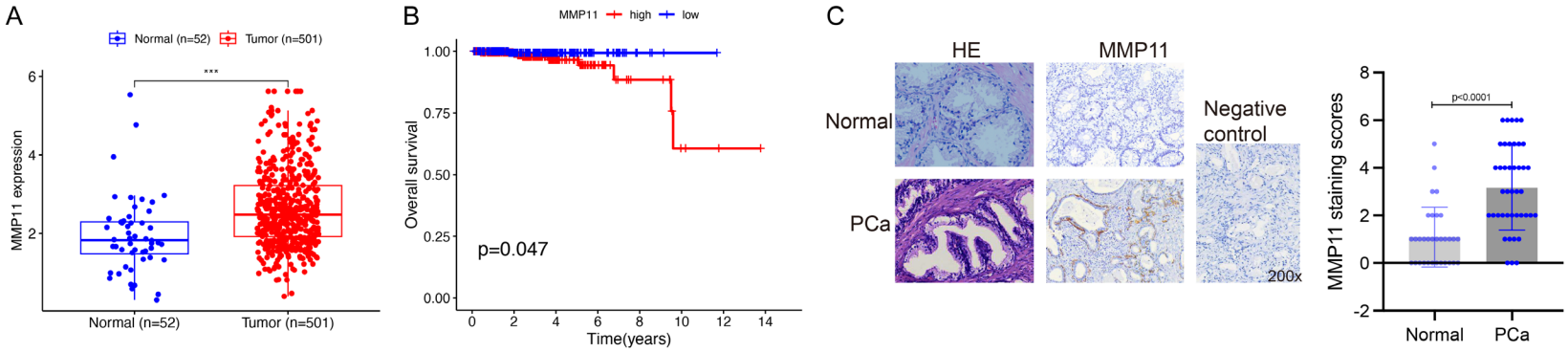

Figure 1. MMP11 expression is increased in clinical PCa specimens vs. normal controls. A. Transcript levels of MMP11 in the TCGA dataset. B. Impact of MMP11 expression on overall survival in PCa patients in the TCGA cohort. C. Protein expression of MMP11 was evaluated by immunohistochemistry in clinicopathological specimens of both PCa and adjacent normal prostate. HE staining showed the tissue morphology (magnification 200 ×). Right: Quantification of MMP11 staining (32 normal samples vs. 42 PCa samples). Data are presented as the means ± SDs. Statistical tests: MMP11 expression analysis, Wilcoxon rank-sum test; survival analysis, log-rank test; MMP11 staining, unpaired Student's t test. ***P < 0.001.

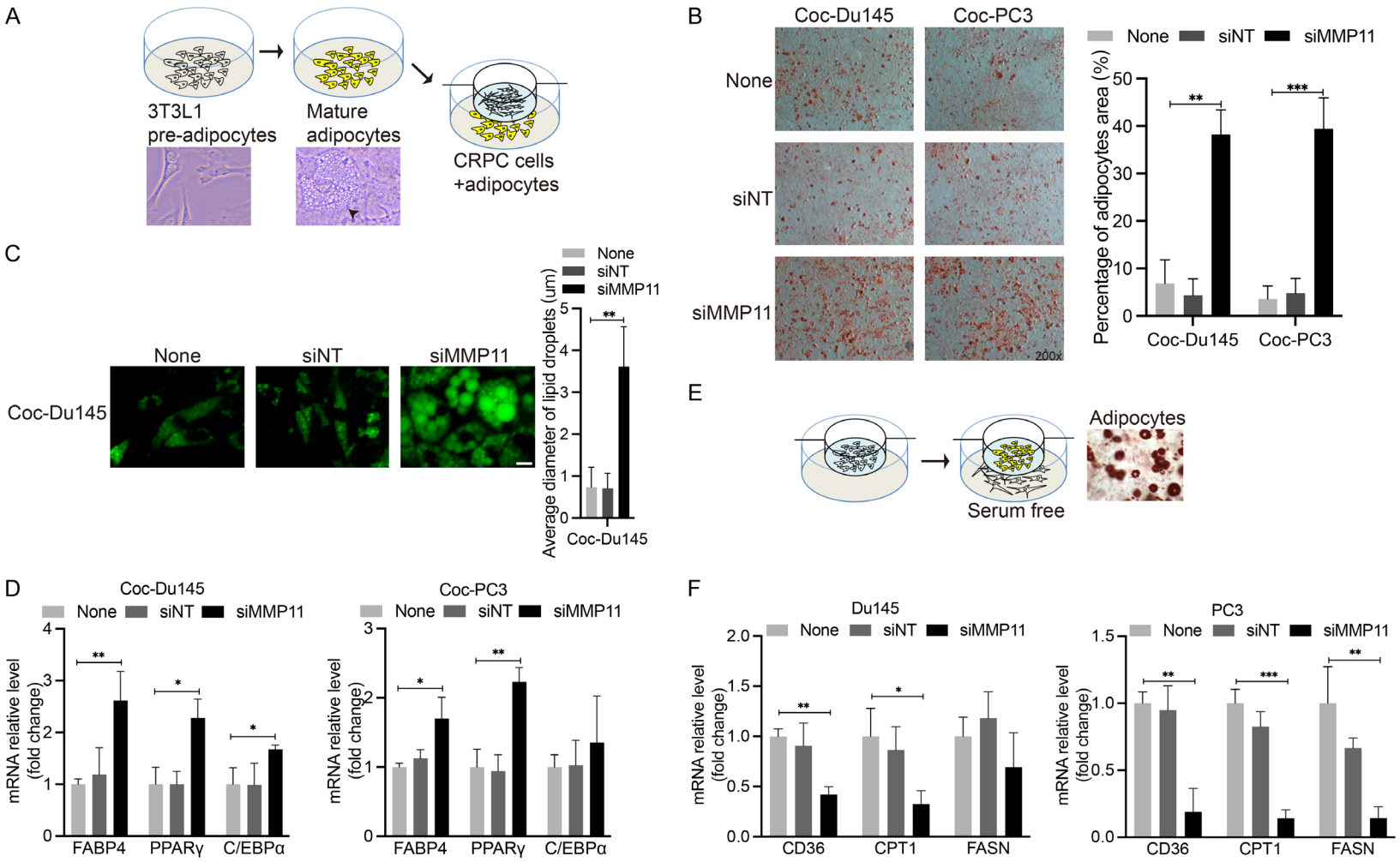

Figure 2. Loss of MMP11 in CRPC cells decreased lipid metabolism and maintained adipocyte maturation in a cell coculture system. A. Schematic diagram showing the coculture model for analyzing adipocytes. The black arrowhead indicates mature adipocytes. B. Cocultured mature adipocytes stained with Oil Red O (magnification 200 ×). Right: Quantification of adipocytes. C. Lipid droplets were labeled with BODIPY in mature adipocytes (scale bar =10 μm). Right: Quantification of lipid droplets. D. The relative mRNA levels of adipocyte differentiation and maturation markers were measured by qPCR. E. Schematic diagram showing the coculture model for analyzing cancer cells. F. The relative mRNA levels of lipid metabolism markers in Du145 and PC3 cells were measured by qPCR. siNT (nontargeting). Data are presented as the means ± SDs. One-way ANOVA followed by Tukey's test; *P < 0.05, **P < 0.01, ***P < 0.001.

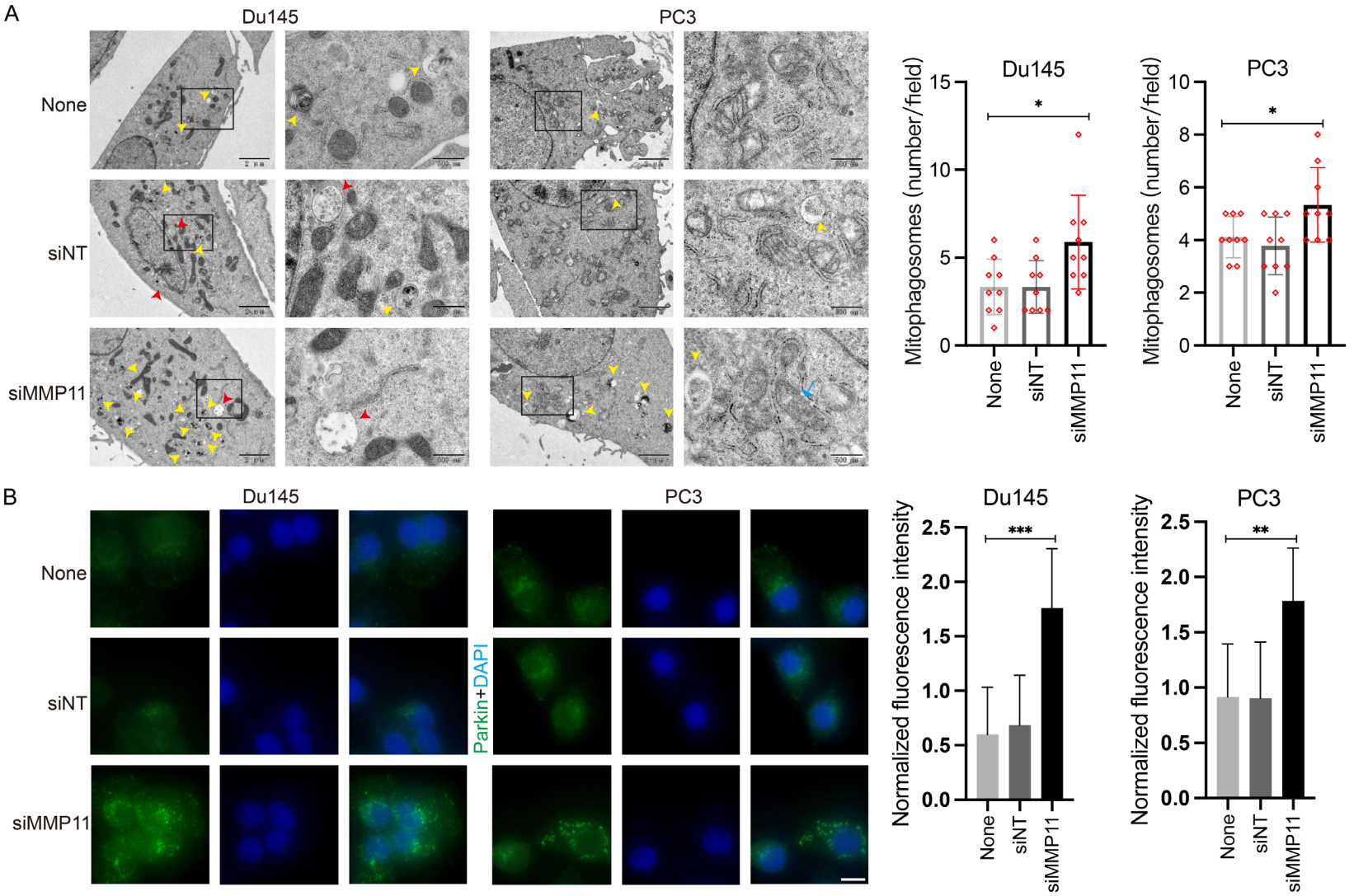

Figure 3. MMP11 deficiency increased mitophagy in CRPC cells. A. Representative electron micrographs of Du145 and PC3 cells are shown. The yellow arrowheads indicate mitophagosomes, the red arrowheads indicate autophagolysosomes, and the blue arrows indicate mitochondrial morphological changes with abnormal cristae or loss of cristae. Right: Quantification of mitophagosomes. B. The mitophagy marker Parkin was detected by immunofluorescence staining (scale bar =10 μm). Right: Quantification of fluorescence intensity. Data are presented as the means ± SDs. One-way ANOVA followed by Tukey's test; *P < 0.05, **P < 0.01, ***P < 0.001.

also correlated with a reduced overall survival (P=0.052) (**Figure 4B**). Intriguingly, combined analysis showed that patients with low expression of both MMP11 and MMP14 had the best overall survival (**Figure 4C**).

To understand the impact of MMP11 and MMP14 on CRPC cell metabolism, we also knocked down MMP14 expression with a MMP14-specific siRNA and used an LC-MS/MS platform to assess the metabolomic profile of control Du145 cells (Du145-C) and Du145 cells with both MMP11 and MMP14 knockdown (Du145-T) (**Figures 5A-D**, S4). The sample qualities were validated (Figure S5). Our results showed that simultaneous deletion of MMP11 and MMP14 in Du145 cells significantly altered the levels of several metabolites (**Figure 5A**). Notably, the levels of metabolites of lipids and lipid-like molecules were significantly decreased in the Du145-T cells compared to the Du145-C cells (**Figure 5B**), suggesting the downregulation of lipid metabolism in MMP11/14 knockdown cells. Furthermore, KEGG analysis was performed to analyze the metabolic pathways in which differential metabolites were enriched and to determine the degree of enrichment (**Figure 5C** and **5D**). Considering that MMP11 is involved in the process of mitophagy, we assessed the mTOR signaling pathway by western blotting, as mTOR is a key regulatory molecule of mitophagy [19]. It was revealed that the mTOR/HIF1α signaling pathway was considerably suppressed by MMP11/14 knockdown (**Figure 5E**). Additionally, CRPC cells also displayed decreased invasion ability based on the decreased MMP2 expression (**Figure 5E** and **5F**).

Silencing MMP11 and MMP14 could attenuate tumor growth by inhibiting lipid metabolism and promoting mitophagy in vivo

We further validated the role of MMP11 and MMP14 in tumor growth by using Du145 cell-derived mouse xenograft tumor model. In consistent with the findings from in vitro study, both the tumor weight and tumor volume were reduced when both MMP11 and/or MMP14 expression was suppressed (**Figure 6A-C**). HE staining revealed the different morphological characteristics of adipocytes between those located near or far from the tumor margin and those in the normal adipose tissue. Specifically, adipocytes near the tumor were smaller and more elongated than distant and normal adipocytes (**Figure 6D**). We further examined the lipid droplets around the tumor by BODIPY staining of the tumor tissue slices and discovered that the lipid accumulation was markedly suppressed in MMP11/14 knockdown cell-derived tumors compared to control cell-derived tumors (**Figure 6E**), suggesting the function of MMP11/14 in lipid uptake. In line with this result, the mRNA levels of FASN and CD36 were also decreased in tumors from MMP11/14 knockdown cells (**Figure 6F**). On the other hand, IHC demonstrated an increased expression of Parkin whereas a decreased expression of Ki67 and MMP2 in tumors from MMP11/14 knockdown cells (**Figure 6G**), supporting the notion that MMP11/14 promotes tumor cell proliferation and invasion by inhibiting mitophagy.

Discussion

Various types of chemokines/cytokines are present in the TME and play different roles during tumor progression. For example, MMP11 is found to suppress tumor apoptosis and alter the mitochondrial unfolded protein response in a mouse breast tumor model [10], while interleukin-22 is reported to increase the metastatic potential of CRPC cells by activating STAT3 [20]. MMP14 is involved in the invasion and metastasis of a wide range of tumors by directly degrading the ECM or indirectly activating MMP2 [21], and the activity of MMP11 may be regulated by MMP14 [15], indicating the complicated network of MMP regulation in the TME. In our TCGA transcriptome analysis, we discovered the opposite expression profiles of MMP11 and MMP14 in PCa tumors compared with normal tissues. Although MMP14 has been reported to be upregulated in cancers [21, 22], we found the transcript level of MMP14 was reduced in PCa tissues in this study. A recent paper demonstrates that adipocytes tend to activate MMP14 expression in human PCa at the invasive front [12]. Interestingly, our two-gene survival analysis based on MMP11 and MMP14 expression indicated that patients in the low MMP11/low MMP14 group had a better prognosis. Indeed, our experimental data revealed that loss of MMP14 augments the tumor-suppressive effect of silencing MMP11 alone via a crosstalk with adipocytes.

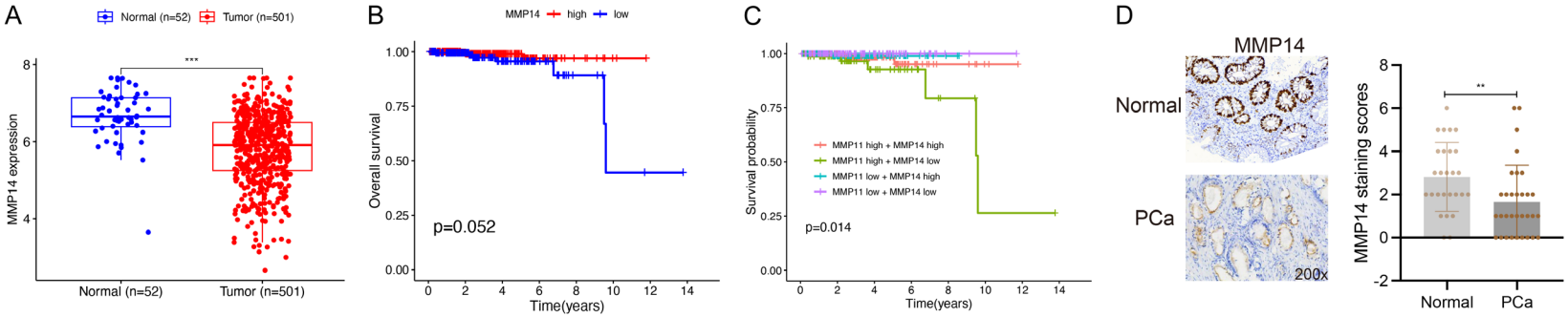

Figure 4. The MMP14 expression level was decreased in clinical PCa specimens. A. Transcript levels of MMP14 in the TCGA dataset. B. Impact of MMP14 expression on overall survival in PCa patients in the TCGA cohort. C. Impact of MMP11 and MMP14 expression on the survival probability in the PCa population. D. The protein expression of MMP14 was evaluated by immunohistochemistry in clinicopathological specimens of both normal and PCa (magnification 200 ×). Right: Quantification of MMP14 staining (27 normal specimens vs. 32 PCa specimens). Data are presented as the means ± SDs. Statistical tests: MMP14 expression, Wilcoxon rank-sum test; survival analysis, log-rank test; MMP14 staining, unpaired Student's t test. **P < 0.01, ***P < 0.001.

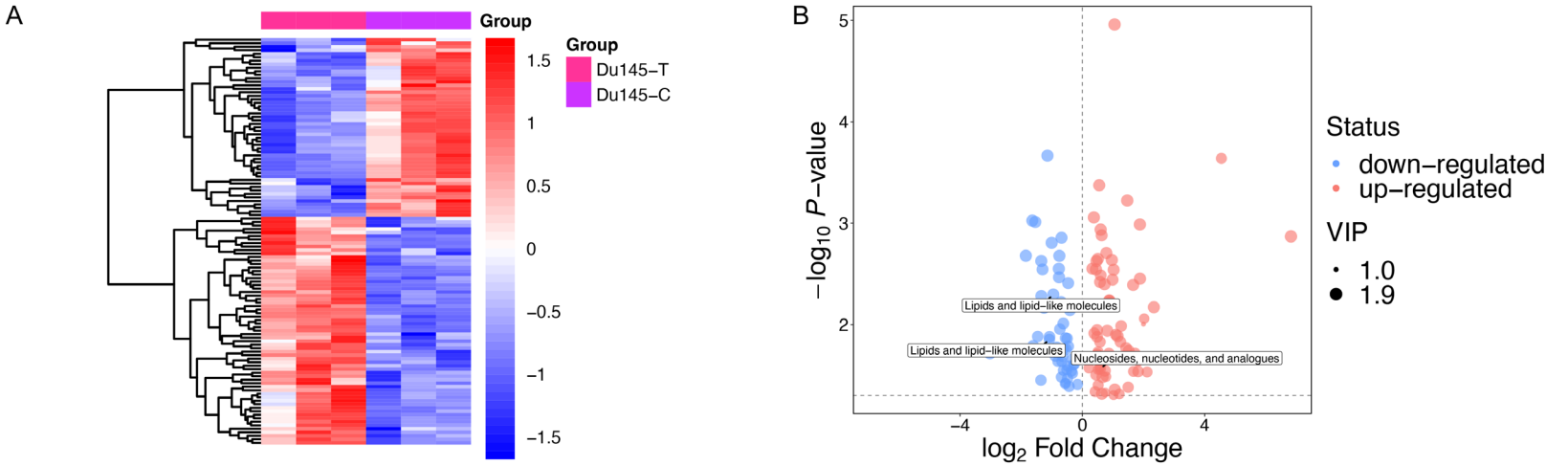

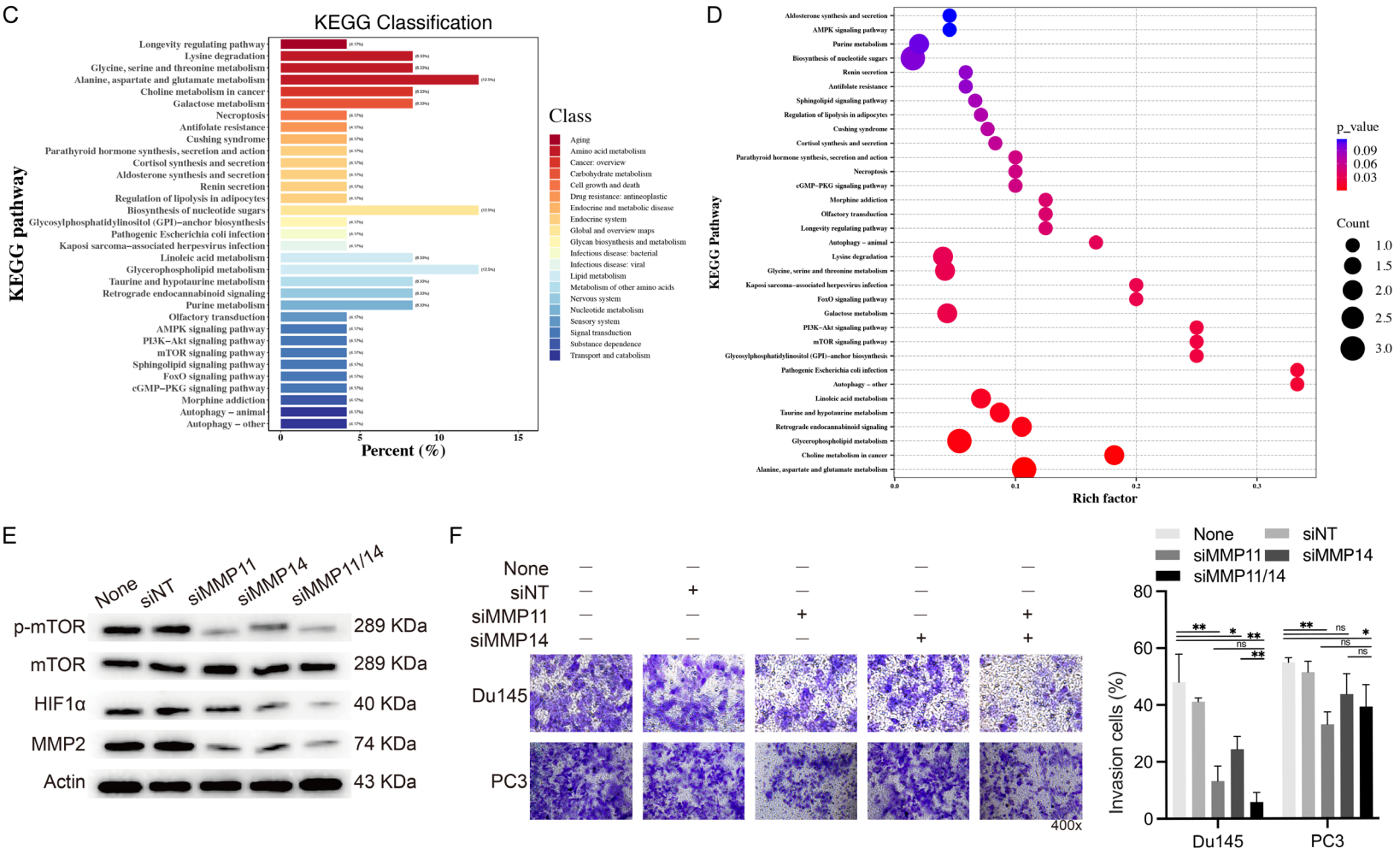

Figure 5. Silencing of MMP11/14 in CRPC cells dramatically inhibited lipid metabolism and cell invasion. (A-D) Data from the Du145-T group (test group, siMMP11/14) vs. the Du145-C group (control group); metabolites with VIP > 1 and P < 0.05 (according to unpaired Student's t test) are shown. Significantly altered metabolites, including lipid and lipid-like molecules, are shown in a heatmap based on hierarchical clustering analysis (A) and in a volcano plot (B). (C, D) The KEGG enrichment analysis results for metabolic pathways are shown for different classifications. (E) The changes in the expression of mTOR/HIF1α/MMP2 signaling pathway molecules involved in Du145 cell lipid metabolism and invasion were further verified by western blotting. (F) A Transwell assay was used to assess the invasive ability of Du145 and PC3 cells after treatment with siMMP11 and siMMP14 (magnification 400 ×). Right: Quantification of invaded cells. Data are presented as the means ± SDs. The invasion assay results were assessed by one-way ANOVA followed by Tukey's test. *P < 0.05, **P < 0.01, ns = not significant.

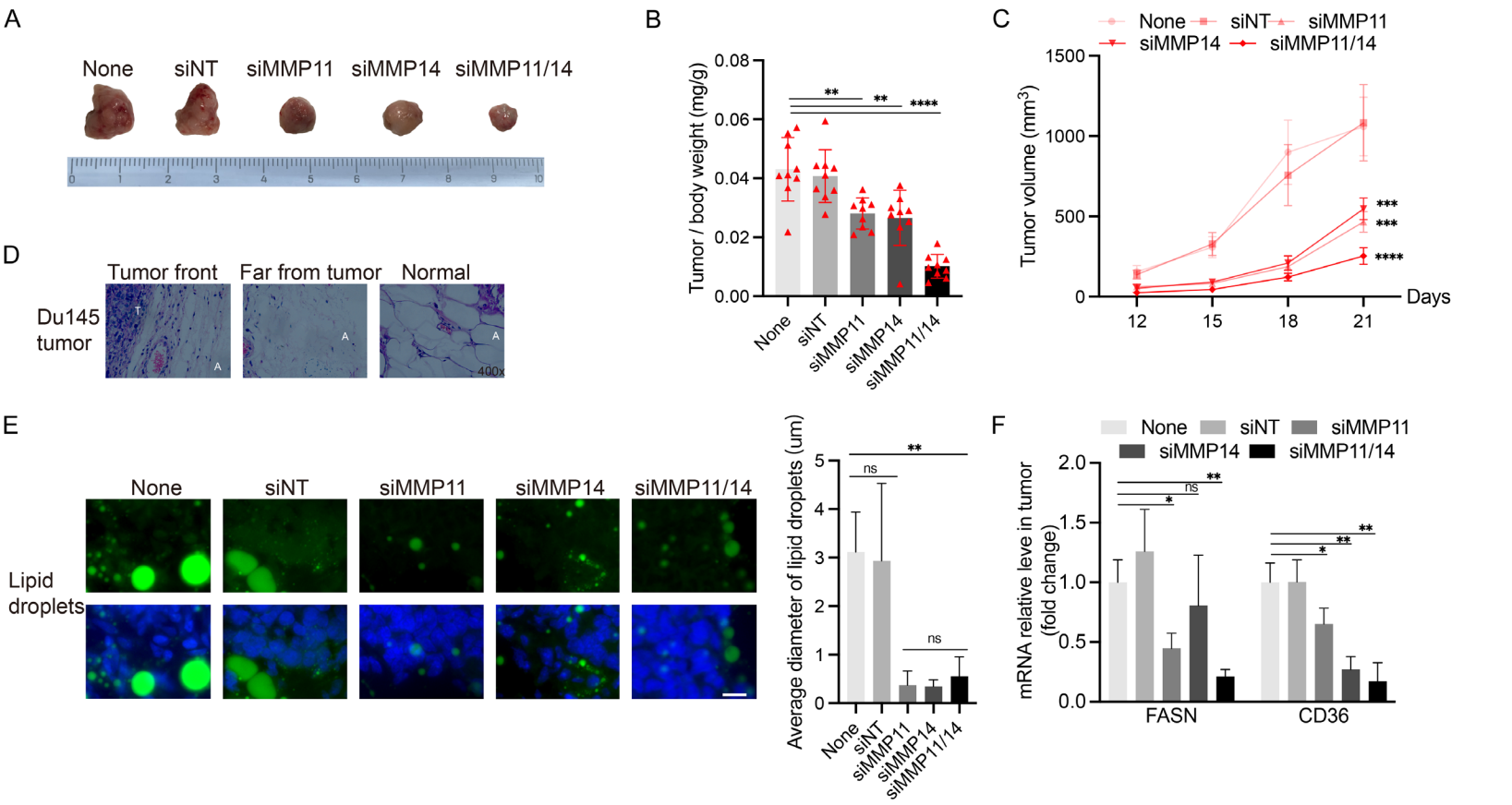
A
None
siNT
siMMP11
siMMP14
siMMP11/14
B
Tumor / body weight (mg/g)
C
Tumor volume (mm3)
Days
D
Tumor front
Far from tumor
Normal
Du145 tumor
400x
E
Lipid droplets
Average diameter of lipid droplets (um)
F
mRNA relative leve in tumor (fold change)
FASN
CD36
G
Parkin
Ki67
MMP2
HE 200x
Negative control
Parkin staining scores
Ki67 staining scores
MMP2 staining scores

Figure 6. Deletion of MMP11/14 delayed Du145 tumor growth in nude mouse models. A. Representative gross appearance of Du145 tumors 21 days after subcutaneous injection of cancer cells. B. Tumor and body weights were measured at the experimental endpoint (21 days). C. Tumor volumes were measured at 12, 15, 18, and 21 days. D. HE staining images of paraffin sections show the size and shape of adipocytes near and far from the tumor, as well as normal adipocytes (magnification 400 ×). T: tumor, A: adipocytes. E. In frozen tissue sections, BODIPY was used to label the lipid droplets around the tumor, and nuclei were labeled with DAPI (scale bar =20 μm). Right: Quantification of lipid droplets. F. The relative mRNA levels of lipid metabolism markers in Du145 tumors were measured by qPCR. G. The protein expression of Parkin, Ki67 and MMP2 was evaluated by immunohistochemical staining of paraffin sections. The HE staining image shows the tumor morphology (magnification 200 ×). Right: Quantification of Parkin, Ki67 and MMP2 staining. Data are presented as the means ± SDs. One-way ANOVA followed by Tukey's test; *P < 0.05, **P < 0.01, ***P < 0.001, ****P < 0.0001, ns = not significant.

Adipocytes function as an energy source for cancer cells, and human omental adipocytes provide FFAs as fuel for rapid tumor growth and invasion in ovarian cancer [23]. In addition, PCa cells have been found to develop stemness properties by the treatment with adipocyte-conditioned medium, and an increased chemoresistance is observed in these cancer cells [24]. Consistent with the notion that these cancer-associated adipocytes (CAAs) exhibit a variety of effects on tumor cells [25], here, we found that downregulation of MMP11 expression in PCa cells significantly reduced delipidation and dedifferentiation in the co-cultured adipocytes. Although the adipocyte morphology did not change noticeably, we observed massive lipid accumulation and increased mRNA levels of the adipocyte maturation markers FABP4 (a carrier protein for FAs) and PPARγ/C/EBPα (adipogenic transcription factors). Moreover, lipid metabolism was significantly decreased in cancer cells, as we observed decreased mRNA levels of CD36, a surface receptor involved in lipid uptake and translocase activity, CPT1, a transporter of long-chain FAs into mitochondria for β-oxidation, and FASN, a lipogenic enzyme for de novo FA synthesis. As expected, the levels of metabolites of lipids and lipid-like molecules were decreased in MMP11/14-silenced CRPC cells. Furthermore, our KEGG pathway enrichment analysis indicated that the mTOR signaling pathway was most likely involved, and this pathway has been reported to promote lipid deposition but suppress mitophagy in macrophages in the context of atherosclerosis [26, 27]. Moreover, deficiency of FFAs and oxygen in the TME regulates the PI3K/AKT/mTOR/HIF-1α pathway and promotes lipogenesis and glycolysis via inhibition of FA β-oxidation in cancer cells [28]. Therefore, we explored the impact of these molecules on PCa cell invasion in our in vitro studies and observed a suppressed mTOR/HIF1α/MMP2 pathway and a decreased cell mobility in MMP11/14 knockdown cells.

Because mitochondria are important organelles that provide energy through FA oxidation via the tricarboxylic acid (TCA) cycle and acetyl-CoA for FA synthesis in the cytosol, it is conceivable that enhancing FA oxidation in mitochondria could regulate Parkin-mediated mitophagy in the context of cardiac dysfunction [29, 30]. Our electron microscopy and immunofluorescence assays showed increased Parkin-mediated mitophagy by MMP11 downregulation. We also observed profound damage to mitochondrial cristae, which is recognized as mitophagy precursor [31, 32], in MMP11 knockdown PC3 cells. In addition to the PINK1-Parkin pathway, other mediators, such as BCL2-interacting protein 3 (BNIP3) and NIP3-like protein X (NIX), can mediate the clearance of damaged mitochondria, but further investigations are needed to clarify the involvement of these factors. Collectively, our results indicate that CRPC cells might undergo metabolic reprogramming and degrade malformed mitochondria into essential substrates for cell survival, probably because the FA supply from neighboring adipocytes is reduced.

Notably, simultaneous silencing MMP14 and MMP11 induced a synergistic inhibitory effect on tumor growth in mice, however, we did not find a significantly less lipid accumulation in the peritumoral space in these mice compared to single knockdown samples. Since previous studies have reported that interactions with adipocytes could activate lipid metabolism in other types of cancer [23], we further verified the expression of the metabolic genes CD36 and FASN and revealed a decreased lipid uptake and synthesis in MMP11 and/or MMP14 knockdown cell-derived tumors. These lipids are essential in providing energy for tumor

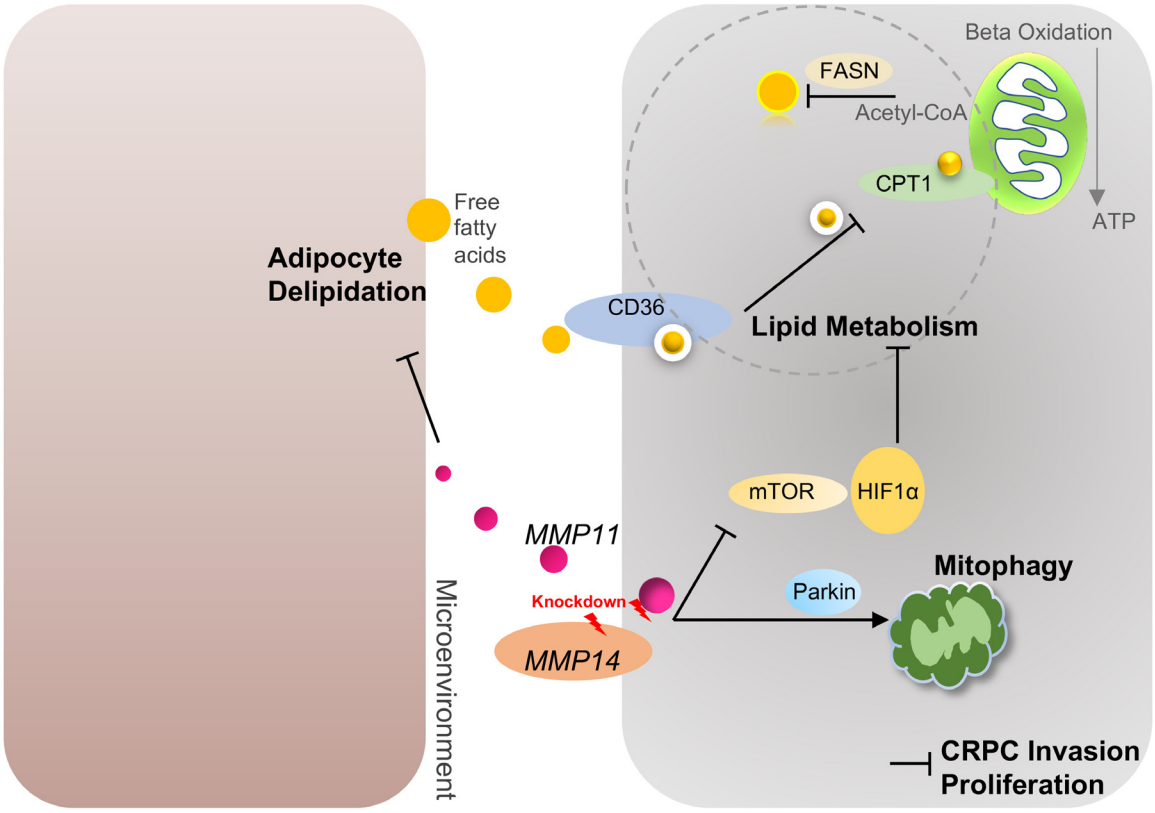

Figure 7. Overview of the proposed role of MMP11 and MMP14 in CRPC cell-adipocyte crosstalk. Adipocyte lipolysis was reduced in the microenvironment by knocking down the expression of the secreted form of MMP11 in CRPC cells, thus decreasing the expression levels of lipid uptake- and metabolism-related genes. Loss of MMP14 augmented the effect of MMP11 absence not only in terms of the reduction in lipid metabolism mediated by the mTOR/HIF1α signaling pathway but also in terms of mitophagy activation induced by Parkin. Thus, these CRPC cells exhibit decreased advantages in proliferation and invasion.

growth and are most likely derived from the CAAs at the tumor front, as these adipocytes display a delipidation phenotype and an elongated fibroblast-like shape. Furthermore, it has been demonstrated that the induction of mitophagy could selectively promote PTEN-negative CRPC cell growth and survival on laminin [33]. In support with this finding, our results showed that knockdown of MMP11 and/or MMP14 not only facilitated mitophagy but also inhibited the proliferation and invasion of PCa cells. Therefore, the synergistic effect of MMP11 and MMP14 downregulation in the TME could lead to a certain extent of benign bilateral crosstalk between adipocytes and CRPC cells.

Conclusions

Knockdown of MMP11 and MMP14 not only inhibited delipidation in neighboring adipocytes, resulting in a lower lipid uptake and metabolism in CRPC cells partially via the mTOR/HIF1α axis, but also increased the level of mitophagy mediated by Parkin, leading to a suppressed growth of CRPC tumors (**Figure 7**). These findings might shed light on developing therapeutic strategies for the intervention of CRPC.

Acknowledgements

This study is supported by the China Postdoctoral Science Foundation (Grant Number: 2022MD723740) and the Natural Science Foundation of Chongqing, China (Grant Number: cstc2021jcyj-msxmX0704).

All patients involved in this study provided informed consent for participation.

Disclosure of conflict of interest

None.

Address correspondence to: Dr. Weiyang He, Department of Urology, The First Affiliated Hospital of Chongqing Medical University, No. 1 Youyi Road, Yuzhong District, Chongqing 400016, China. E-mail: weiyangh361@163.com

References

[1] Teo MY, Rathkopf DE and Kantoff P. Treatment of advanced prostate cancer. Annu Rev Med 2019; 70: 479-499.

[2] Kim SJ, Park MU, Chae HK, Nam W, Kim SW, Yu H, Kim HG, Kang GH and Park JY. Overweight and obesity as risk factors for biochemical recurrence of prostate cancer after radical prostatectomy. Int J Clin Oncol 2022; 27: 403-410.

[3] Keto CJ, Aronson WJ, Terris MK, Presti JC, Kane CJ, Amling CL and Freedland SJ. Obesity is associated with castration-resistant disease and metastasis in men treated with androgen deprivation therapy after radical prostatectomy: results from the SEARCH database. BJU Int 2012; 110: 492-498.

[4] Tiwari A, Trivedi R and Lin SY. Tumor microenvironment: barrier or opportunity towards effective cancer therapy. J Biomed Sci 2022; 29: 83.

[5] Rybinska I, Mangano N, Tagliabue E and Triulzi T. Cancer-associated adipocytes in breast cancer: causes and consequences. Int J Mol Sci 2021; 22: 3775.

[6] de Almeida LGN, Thode H, Eslambolchi Y, Chopra S, Young D, Gill S, Devel L and Dufour A. Matrix metalloproteinases: from molecular mechanisms to physiology, pathophysiology, and pharmacology. Pharmacol Rev 2022; 74: 712-768.

[7] Ma B, Ran R, Liao HY and Zhang HH. The paradoxical role of matrix metalloproteinase-11 in cancer. Biomed Pharmacother 2021; 141: 111899.

[8] Escaff S, Fernández JM, González LO, Suárez A, González-Reyes S, González JM and Vizoso FJ. Study of matrix metalloproteinases and their inhibitors in prostate cancer. Br J Cancer 2010; 102: 922-929.

[9] Hsieh CY, Chou YE, Lin CY, Wang SS, Chien MH, Tang CH, Lin JC, Wen YC and Yang SF. Impact of matrix metalloproteinase-11 gene polymorphisms on biochemical recurrence and clinicopathological characteristics of prostate cancer. Int J Environ Res Public Health 2020; 17: 8603.

[10] Tan B, Jaulin A, Bund C, Outilaft H, Wendling C, Chenard MP, Alpy F, Cicek AE, Namer IJ, Tomasetto C and Dali-Youcef N. Matrix metalloproteinase-11 promotes early mouse mammary gland tumor growth through metabolic reprogramming and increased IGF1/AKT/FoxO1 signaling pathway, enhanced ER stress and alteration in mitochondrial UPR. Cancers (Basel) 2020; 12: 2357.

[11] Zhong J, Shan W and Zuo Z. Norepinephrine inhibits migration and invasion of human glioblastoma cell cultures possibly via MMP-11 inhibition. Brain Res 2021; 1756: 147280.

[12] Laurent V, Toulet A, Attané C, Milhas D, Dauvillier S, Zaidi F, Clement E, Cinato M, Le Gonidec S, Guérard A, Lehuédé C, Garandeau D, Nieto L, Renaud-Gabardos E, Prats AC, Valet P, Malavaud B and Muller C. Periprostatic adipose tissue favors prostate cancer cell invasion in an obesity-dependent manner: role of oxidative stress. Mol Cancer Res 2019; 17: 821-835.

[13] Sakamoto T, Weng JS, Hara T, Yoshino S, Kozuka-Hata H, Oyama M and Seiki M. Hypoxia-inducible factor 1 regulation through cross talk between mTOR and MT1-MMP. Mol Cell Biol 2014; 34: 30-42.

[14] Sakamoto T and Seiki M. A membrane protease regulates energy production in macrophages by activating hypoxia-inducible factor-1 via a non-proteolytic mechanism. J Biol Chem 2010; 285: 29951-29964.

[15] Buache E, Thai R, Wendling C, Alpy F, Page A, Chenard MP, Dive V, Ruff M, Dejaegere A, Tomasetto C and Rio MC. Functional relationship between matrix metalloproteinase-11 and matrix metalloproteinase-14. Cancer Med 2014; 3: 1197-1210.

[16] Yang JH, Kim NH, Yun JS, Cho ES, Cha YH, Cho SB, Lee SH, Cha SY, Kim SY, Choi J, Nguyen TM, Park S, Kim HS and Yook JI. Snail augments fatty acid oxidation by suppression of mitochondrial ACC2 during cancer progression. Life Sci Alliance 2020; 3: e202000683.

[17] Mukherjee S, Bhatti GK, Chhabra R, Reddy PH and Bhatti JS. Targeting mitochondria as a potential therapeutic strategy against chemoresistance in cancer. Biomed Pharmacother 2023; 160: 114398.

[18] Tan HWS, Lu G, Dong H, Cho YL, Natalia A, Wang L, Chan C, Kappei D, Taneja R, Ling SC, Shao H, Tsai SY, Ding WX and Shen HM. A degradative to secretory autophagy switch mediates mitochondria clearance in the absence of the mATG8-conjugation machinery. Nat Commun 2022; 13: 3720.

[19] Lahiri V, Hawkins WD and Klionsky DJ. Watch what you (self-) eat: autophagic mechanisms that modulate metabolism. Cell Metab 2019; 29: 803-826.

[20] Tan B, Chen X, Fan Y, Yang Y, Yang J and Tan L. STAT3 phosphorylation is required for the HepaCAM-mediated inhibition of castration-resistant prostate cancer cell viability and metastasis. Prostate 2021; 81: 603-611.

[21] Poincloux R, Lizárraga F and Chavrier P. Matrix invasion by tumour cells: a focus on MT1-MMP trafficking to invadopodia. J Cell Sci 2009; 122: 3015-3024.
[22] Dong Y, Chen G, Gao M and Tian X. Increased expression of MMP14 correlates with the poor prognosis of Chinese patients with gastric cancer. Gene 2015; 563: 29-34.
[23] Nieman KM, Kenny HA, Penicka CV, Ladanyi A, Buell-Gutbrod R, Zillhardt MR, Romero IL, Carey MS, Mills GB, Hotamisligil GS, Yamada SD, Peter ME, Gwin K and Lengyel E. Adipocytes promote ovarian cancer metastasis and provide energy for rapid tumor growth. Nat Med 2011; 17: 1498-1503.
[24] Fontana F, Anselmi M and Limonta P. Adipocytes reprogram prostate cancer stem cell machinery. J Cell Commun Signal 2023; 17: 915-924.
[25] Yao H and He S. Multi-faceted role of cancer-associated adipocytes in the tumor microenvironment (Review). Mol Med Rep 2021; 24: 866.
[26] Banerjee D, Sinha A, Saikia S, Gogoi B, Rathore AK, Das AS, Pal D, Buragohain AK and Dasgupta S. Inflammation-induced mTORC2-Akt-mTORC1 signaling promotes macrophage foam cell formation. Biochimie 2018; 151: 139-149.
[27] Zhang X, Sergin I, Evans TD, Jeong SJ, Rodriguez-Velez A, Kapoor D, Chen S, Song E, Holloway KB, Crowley JR, Epelman S, Weihl CC, Diwan A, Fan D, Mittendorfer B, Stitziel NO, Schilling JD, Lodhi IJ and Razani B. High-protein diets increase cardiovascular risk by activating macrophage mTOR to suppress mitophagy. Nat Metab 2020; 2: 110-125.
[28] Weinstein AG, Godet I and Gilkes DM. The rise of viperin: the emerging role of viperin in cancer progression. J Clin Invest 2022; 132: e165907.
[29] Nowinski SM, Solmonson A, Rusin SF, Maschek JA, Bensard CL, Fogarty S, Jeong MY, Lettlova S, Berg JA, Morgan JT, Ouyang Y, Naylor BC, Paulo JA, Funai K, Cox JE, Gygi SP, Winge DR, DeBerardinis RJ and Rutter J. Mitochondrial fatty acid synthesis coordinates oxidative metabolism in mammalian mitochondria. Elife 2020; 9: e58041.
[30] Shao D, Kolwicz SC Jr, Wang P, Roe ND, Villet O, Nishi K, Hsu YA, Flint GV, Caudal A, Wang W, Regnier M and Tian R. Increasing fatty acid oxidation prevents high-fat diet-induced cardiomyopathy through regulating parkin-mediated mitophagy. Circulation 2020; 142: 983-997.
[31] Small DM, Morais C, Coombes JS, Bennett NC, Johnson DW and Gobe GC. Oxidative stress-induced alterations in PPAR-γ and associated mitochondrial destabilization contribute to kidney cell apoptosis. Am J Physiol Renal Physiol 2014; 307: F814-822.
[32] Lin YC, Lin YC, Tsai ML, Liao WT and Hung CH. TSLP regulates mitochondrial ROS-induced mitophagy via histone modification in human monocytes. Cell Biosci 2022; 12: 32.
[33] Nollet EA, Cardo-Vila M, Ganguly SS, Tran JD, Schulz VV, Cress A, Corey E and Miranti CK. Androgen receptor-induced integrin α6β1 and Bnip3 promote survival and resistance to PI3K inhibitors in castration-resistant prostate cancer. Oncogene 2020; 39: 5390-5404.

Table S1. Sequences of Primers and siRNAs

Names	Sense (5'-3')	Antisense (5'-3')	Species
Sequences of Primers			
GAPDH	AGGTCGGTGTGAACGGATTTG	TGTAGACCATGTAGTTGAGGTCA	Mu/Hu
FABP4	AAGGTGAAGAGCATCATAACCCT	TCACGCCTTTCATAACACATTCC	Mu
PPARγ	TCGCTGATGCACTGCCTATG	GAGAGGTCCACAGAGCTGATT	Mu
C/EBPα	CAAGAACAGCAACGAGTACCG	GTCACTGGTCAACTCCAGCAC	Mu
CD36	AAGCCAGGTATTGCAGTTCTTT	GCATTTGCTGATGTCTAGCACA	Hu
CPT1	TTTGCCTCGTGTTTGTGGG	CAGCCGTGGTAGGACAGAA	Hu
FASN	ACAGCGGGGAATGGGTACT	GACTGGTACAACGAGCGGAT	Hu
Sequences of siRNAs			
siNT	UUCUCCGAACGUGUCACGU	ACGUGACACGUUCGGAGAA	Hu
siMMP11	GUCCAUGCUGCCUUGGUCU	AGACCAAGGCAGCAUGGAC	Hu
siMMP14	GCAAAUUCGUCUUCUUCAA	UUGAAGAAGACGAAUUUGC	Hu

Table S2. Primary and secondary antibodies

Names	Applications	Sources	Distributors
Primary antibodies			
p-mTOR	WB, 1:1000	Rabbit	#5536, CST
mTOR	WB, 1:1000	Rabbit	#2983, CST
HIF1α	WB, 1:1000	Mouse	AG2135, Beyotime
Ki67	IHC, 1:500	Rabbit	60738R, Bioss
Parkin	IHC, 1:100; IF, 1:200	Rabbit	ET1702-60, Huabio
MMP11	WB, 1:500; IHC, 1:50	Rabbit	ET1611-33, Huabio
MMP14	WB, 1:1000; IHC, 1:100	Rabbit	ET1606-48, Huabio
MMP2	WB, 1:1000; IHC, 1:500	Rabbit	YT2798, Immunoway
β-actin	WB, 1:2000	Mouse	YM3028, Immunoway
Secondary antibodies			
Anti-rabbit IgG	WB, 1:1000; IHC, 1:200	Goat	A0208, Beyotime
Anti-mouse IgG	WB, 1:1000; IHC, 1:200	Goat	A0216, Beyotime
Anti-rabbit AlexaFluor 488	IF, 1:1000	Goat	0295P, Bioss

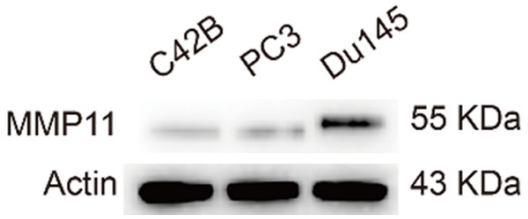

Figure S1. Du145 and PC3 cells express higher levels of MMP11 protein than C42B cells.

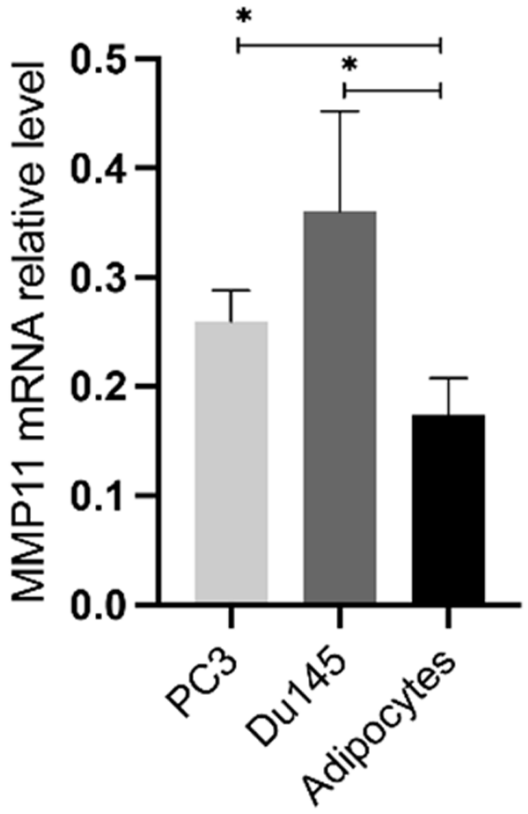

Figure S2. Du145 and PC3 cells express significantly higher levels of endogenous MMP11 mRNA than adipocytes. One-way ANOVA followed by Tukey's test; *P < 0.05.

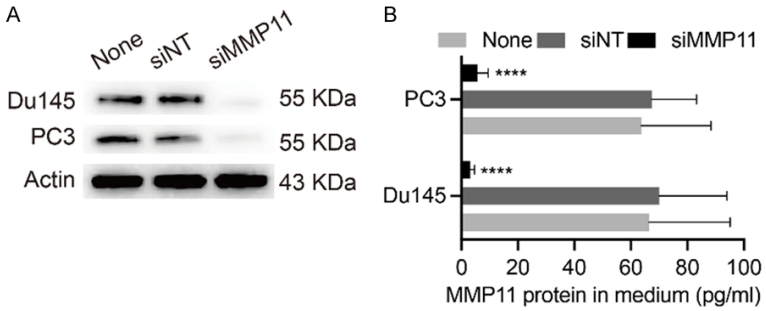

Figure S3. The MMP11 protein levels in CRPC cells and the culture medium were reduced by a targeted siRNA. A. MMP11 protein expression was inhibited by a targeted siRNA in Du145 and PC3 cells. B. The absence of MMP11 in Du145 and PC3 cells led to a significant decrease in the protein content in the cell culture medium. One-way ANOVA followed by Tukey's test; ****P < 0.0001.

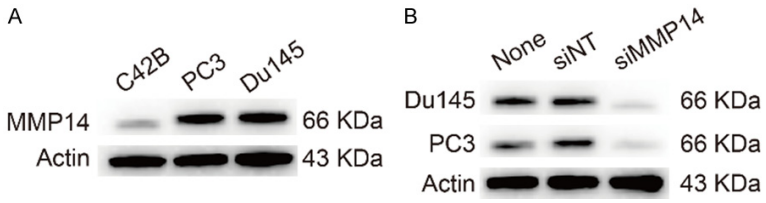

Figure S4. MMP14 protein expression was reduced by a targeted siRNA in CRPC cells. A. MMP14 protein expression in C42B, PC3 and Du145 cells. B. MMP14 expression was inhibited by the targeted siRNA in Du145 and PC3 cells.

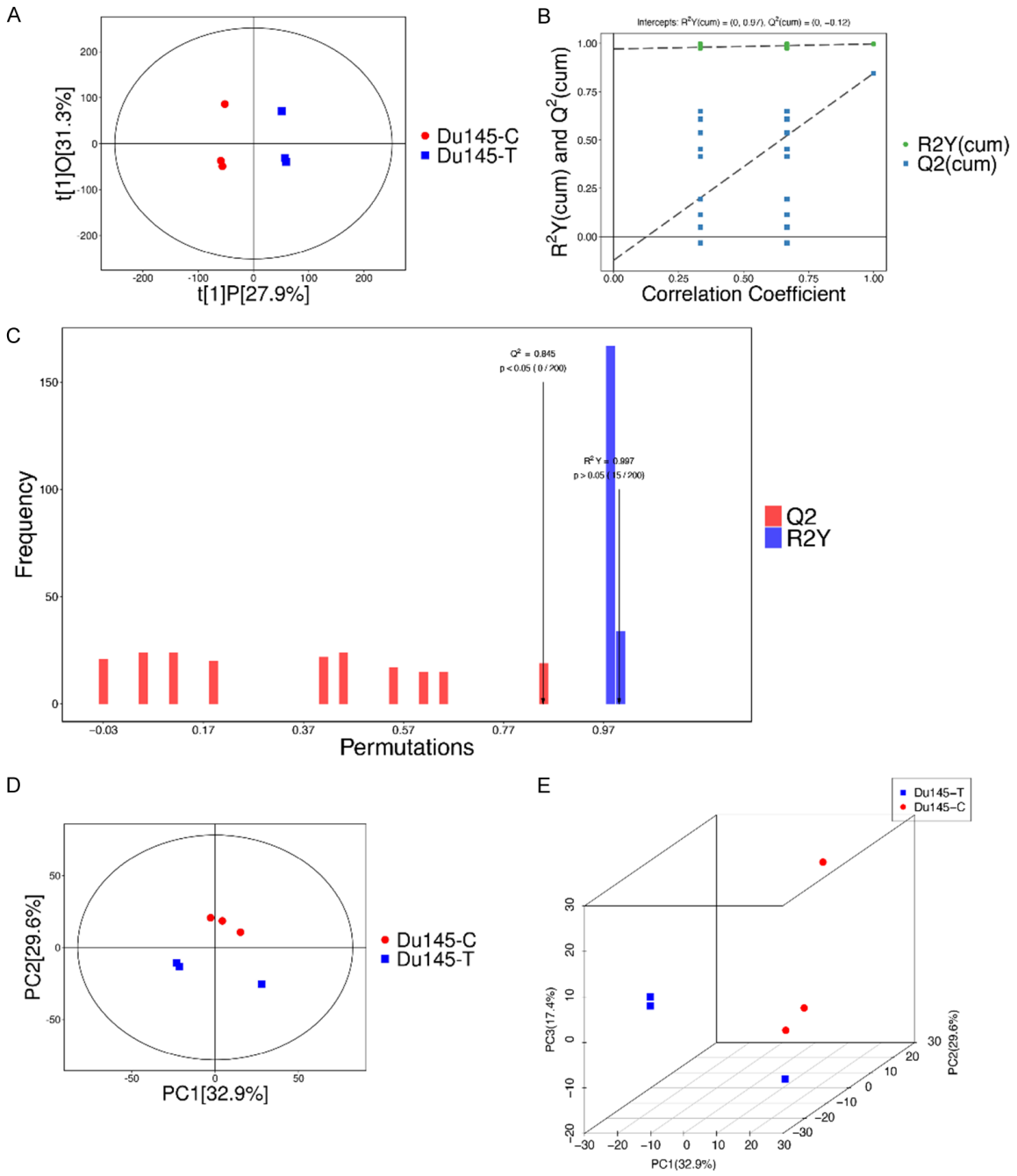

Figure S5. Metabolomic samples were evaluated for overall quality (Du145-T vs. Du145-C). A. Scatter plot of OPLS-DA scores. B. Permutation plot for the OPLS-DA model. C. Permutation histogram for the OPLS-DA model. D. Scatter plot of PCA scores. E. 3D PCA score plot.